FRICTION AND WEAR OF CARBON-CARBON COMPOSITE
PART 2: TEMPERATURE AND STRESS FIELDS ANALYSIS

Kia-Moh Teo and Khalid Lafdi
NSF-University-Industry
Center For Advanced Friction Studies,
Southern Illinois University at Carbondale, IL. 62901-4343, *lafdi@siu.edu*

Introduction

During a rubbing process, interaction between frictional heating, thermal distortion and contact mechanism may cause the development of non-uniform contact pressure and thermal instability [1]. The generation of hot spots on the friction surface may cause material degradation and thermal stress failure. The effect of load and speed on the maximum temperature was discussed by Barber et al. [2]. They reported that an increase in speed might cause a reduction of contact area and hence increase the hot spotting temperature. It was found that in most braking system, the periodic heating and loading of brakes would influence thermal and contact stress fields differently.

The analysis of temperature field on the friction surface is very complicated due to the high thermal gradient at the interface and the high flash temperature of contact asperity which last for only a fraction of a second [2,3]. Moreover, the determination of heat partition factor is very complex. Some researchers found that the partition factor is dependent on thermal conductivity ratio [4]. Dry sliding friction was determined to have two basic factors: interfacial bond and material deformation [5,6]. Adhesive bond at the interface is said to be the main factor of frictional energy.

Kimura et al. reported that the coefficient of friction of carbon brakes increases with increasing heat treatment and Young's modulus [7]. They found that the wear of composites for coefficient of friction above 0.4 is dominated by an abrasion mechanism. There are two types of surface morphology observed on carbon-carbon composites' friction surfaces, which are due to the contact pressure differences. These pressure differences play an important role in the stress field of the brakes.

During manufacturing of brake disk, residual stresses will develop in the structural materials. It is believed that when the disk brake rotors overheat, changes in residual stresses in the disks might cause them to distort and vibrate. To reduce thermal distortion or thermal fade, overheating has to be avoided. Ventilation is one of the ways to reduce thermal fade by convection. However, ventilation will enhance oxidation of carbon brakes [8]. It appears then the study of temperature and stress fields of carbon brake become important for better performance.

Temperature field analysis

During any friction and wear process, a significant amount of heat is generated between the two sliding surfaces. Depending on the material properties, sliding velocity, contact nature, rubbing geometry and mass, the heat flux generated on the friction interface will be partitioned among the rotor and stator [9]. Determination of the heat partition factor is extremely complicated [10]. For identical materials of similar geometry, it is commonly considered that the heat is shared equally between the rotor and stator. Further simplification includes total conversion of kinetic energy to heat. In reality, kinetic energy can be converted by means of friction to heat, sound, vibration, chemical energy and wear of materials.

To model the temperature field of the sample, we need to determine how much heat is diffused into the sample. A conventional way to determine this heat partition is by assuming equal division. However, other alternative methods can be considered to approximate this heat more accurately. Since the mass of the stator sample used in the fast test is quite small, has high thermal conductivity and if the back of the sample is thermally insulated, the thermal gradient in the sample is expected to be small. This makes a general lumped capacitance method applicable for preliminary approximation for the heat flux. In general, the thermal energy in the sample can be represented as follows:

$$\dot{E}_{in} = \dot{E}_{out} + \dot{E}_{stored} \qquad \text{(a)}$$

$$Q(t) = hA(T - T_{amb}) + \sigma\varepsilon A(T^4 - T_{sur}^4) + \rho c_p V\frac{dT}{dt} \qquad \text{(b)}$$

where Q is the heat absorbed by the sample, h is the convection coefficient of the ambient air, A is the contact area, σ is the Stefan-Boltzmann constant, ε is emissivity of the sample, T is the temperature recorded by the thermocouple, T_{amb} is the ambient temperature, T_{sur} is the surrounding temperature, and ρ, c_p and V is the density, specific heat and volume of the sample, respectively.

Knowing the thermal transport properties of the sample and the environmental conditions, a heat energy balance can be established. This energy balance will contribute to determine friction heat rate as function of time, Q(t). Thermal properties of the sample such as thermal diffusivity and specific heat were measured experimentally in our laboratory and are illustrated in Figure 1.

Heat losses due to convection and radiation are also included in the estimation. By providing appropriate insulation at the back of the sample holder, conduction heat loss to the sample holder is minimized and therefore can be neglected. In our model, convection coefficient is taken to be 25 $W/m^{2o}C$ from literature [11]. Coke's emissivity is taken as 0.9, as for most carbon materials. The energy stored in the sample can be calculated from temperature history of the sample. In this work, a thermocouple is placed into the sample 2.5 mm from the rubbing surface. Carbon paint is used to provide good thermal contact between the junction and the sample. The response of the thermocouple is recorded using a data logger. Figure 2 shows the temperature history of the sample for the entire 90 minutes test along with its numerical gradient, dT/dt. By substituting all known parameters mentioned before into equation (b), friction heat rate to the sample can be calculated as a function of time. Figure 3a shows the heat flux diffusing into the sample as function of time.

The apparent contact area between the sample and disk observed to change during friction transitions. The degree of change can be estimated by the fingerprints or traces of the wear tracks that were created on the sliding surface. As shown in the Figure 3a, the heat flux tends to increase during the transition. It is also found that only 1% to 30% of the friction energy is converted into heat and absorbed by the sample (Figure 3b) Most of the rest of the friction energy is absorbed by the rotor disk.

To simulate the temperature field in the sample, a finite element mesh comprised of brick elements with eight nodes and a single degree of freedom (temperature) was generated as shown in Figure 4.In the model, the four outer faces of the model is subjected to convection. However, the back surface of the model (and the actual sample) is fully insulated. Various heat fluxes were applied to the friction surface. The temperature simulated at the location of the thermocouple along with the heat fluxes applied to the model is shown in Figure 5.

It is clearly shown that temperature increases very fast in the beginning of friction process and at the initiation of a transition. Both the numerical simulation and experimetal results compare favorably. The simulation has been made based on two combined effects: the rate of heat absorption as a function of time and the observed actual contact area calculated from the wear tracks. Figure 6 shows the predicted temperature field of the sample at specific times during the friction test. We notice that during the transition, heat is localised along the wear track due to the observed decrease in contact area, and its impact on the temperatue magnitude becomes greater as the test progresses.

Stress field analysis

During sliding, thermal stress gradients may be generated within the sample and these gradients may produce cracks. To study and simulate the stress field, generated within the sample, thermal and mechanical properties of the sample must be known. Figure 7 shows the mechanical properties used in the analysis as functions of temperature. The properties at room temperature were taken from literature [12,13]. It is assumed that these properties decrease exponentially with increasing temperature. The thermal expansion characteristics of the sample were given in Figure 1. It is also assumed that the sample has a Poisson's ratio of 0.3 for the whole range of temperature. Flexural and compressive strengths of the sample range from 10 to 120 MPa and from ~10 to 40 MPa respectively at room temperature from literature [12,13].

To predict the thermal stress, the temperature field of the complete model was computed. The temperature from this complete model was then applied to a finite element mesh (complete model mesh) that are comprised of structural brick element with three degree of freedoms (translation x, y and z). Since the sample is clamped to the loading arm of the FAST machine, the back surface of the model is fully constrained. Coupled with the friction shear and normal pressure, a complete thermo-elastic stress field of the sample is simulated. Since the sample is tested under constant friction force, the shearing force applied to the model is also constant. Figure 8 shows a typical variation of normal force and the coefficient of friction as a function of time.

It is observed that during the friction transition, wear tracks are created. During the first and second transitions, the wear tracks appeared at the same locations on the disk. These wear tracks reveal that during the transitions, the contact pressure and friction shear are localized along the tracks. Figure 9 shows the predicted von-mises stress (distortional energy density) field of the sample at each specific time during the test.

From the stress analysis, it is found that at the beginning of the friction process the stress is fairly low. Higher stresses are located along the back bottom edge of the sample. As the time increases, stresses start to build up mainly due to the increasing normal pressure when friction film is formed. When the first friction transition occurs, stresses at the end of the wear track increase. As the transition progresses, maximum stress increases to a value of 11.887 MPa at the bottom edge of the friction surface. Comparing this value to the strengths of the sample, crack is expected to occur and propagate into the sample from this location. This crack is caused by the higher contact pressure and thermal stresses. Creation of the cracks will vary the nature (mechanical strength and structure) of the sample and causes the prediction of the stress to deviate from the real situation. Figure 2-32 below shows the cracks created at the end of wear tracks of the samples after the FAST tests.

Conclusions

In general, we found that the evolution of a friction transition is closely related to the rate of the energy absorbed and the friction film. Stress may develop on the surface and within the bulk material. The friction film can be disrupted by this stress. The disruption of the friction film creates wear tracks, which made up of debris. The shearing of these particulates cause both friction and thermal instabilities. Friction surfaces of the sample were examined using various techniques. A structural change from graphitic to amorphous carbon has occurred on the surface of the specimen. During the run-in process, a friction film is built up. Apart from the water effect (water was desorbed at high power input), the shear stress within the film increases during a friction transition and causes an increase in the friction coefficient. The stresses increase until it disrupts the film and causes a sudden change in friction coefficient. However, the disruption of the film releases the wear particulates and caused a decrease in true contact area. Decrease of contact area keeps the friction coefficient high but decreases gradually as film is being built again. The shear stress may propagate and crack the bulk material.

Temperature and stress fields of the sample were simulated for the entire test period. It was found that only about 1% to 30% of the friction heat was absorbed by the sample. Temperature was very localized along the wear tracks during transitions. Analysis from stress field simulation shows that cracks tend to occur at the bottom edge of the wear track. The study shows that any type of failure (mechanical or thermal fatigue) of the friction film or bulk material was sufficient to generate either a frictional transition or a thermal instability.

References

1. Barber, J. R., Beamond, T.W., Waring, J. R. and Pritchard, C., 1985, "Implications of Thermoelastic Instability for the Design of Brakes." Transaction of the ASME, 107, pp. 206-210.
2. Zaidi, H., 1998, Thesis INPL, Nancy, France.
3. Archard, J. F., 1958, Wear, 2, pp. 438..
4. Zaidi, H. and Senouci, A., 1999, "Thermal Tribological Behavior of Composite Carbon Metal/Steel Brake." Applied Surface Science, 144-145, pp. 265-271.
5. Kragelskii, I. V., 1965, Friction and Wear. Butterworths, London.
6. Tabor, D., 1981, " Friction – the Present State of our Understanding." J. Lubr. Tech. 103, pp. 169-179.
7. Kimura, S., Yasuda, E., Narita, N., 1984, JSLE, Int. Ed. 5, pp. 11-16.
8. Savage, G., 1993, Carbon-Carbon Composites, Chapman & Hall, London, pp. 323-346.
9. Blok, H., 1937, "Theoretical Study of Temperature Rise at Surfaces of Actual Contact under oiliness Lubricating Conditions." Proc. Inst. Of Mechanical Engineers: General Discussion of Lubrication, 2, pp. 222-235 [Institution of Mechanical Engineers, London].
10. Ling, F.F., 1973, Surface Mechanics, Wiley.
11. Incropera, F. P. and Dewitt, D. P., 1996, Introduction to Heat Transfer, 3 Ed., Wiley, pp. 8.
12. Losty, H. H. W., 1970, Mechanical Properties in Modern Aspects of Graphite Technology, Academy Press, N. Y.
13. Girard, H. and Slonia, J. P., 1978, proc. 5th Int. Conf. On Carbon and Graphite, 1, pp. 483.

Figure 1. Thermal properties of sintered coke carbonized to 2200 ^{o}C as function of temperature.

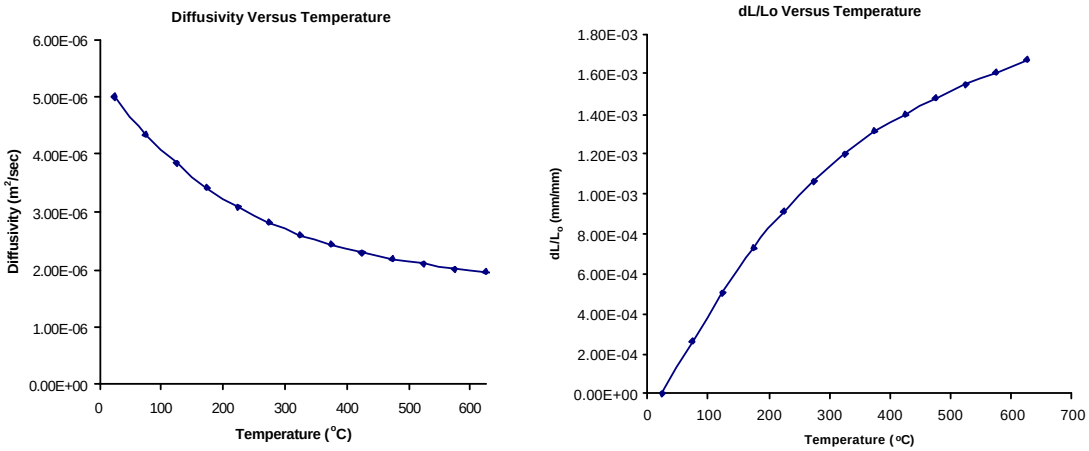

Figure 2. Temperature history of the sample for 90 minutes test period at 69.74 N and 850 rpm.

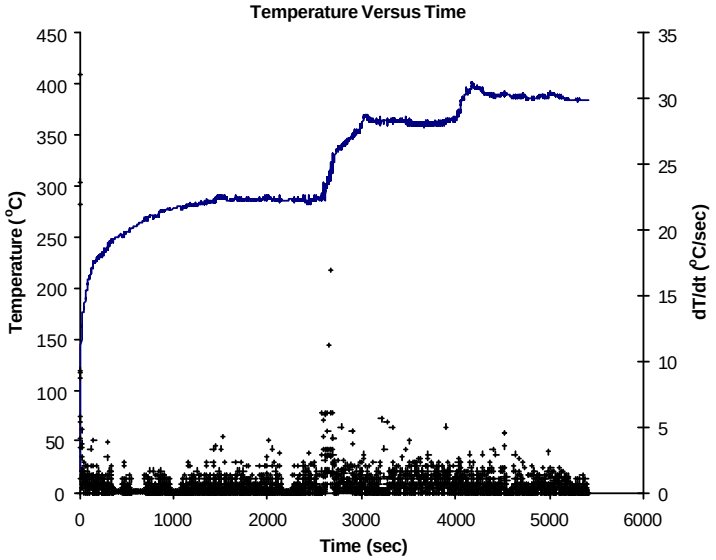

Figure 3. Fiction heat flux absorbed by the sample as a function of time (a) Heat flux and temperature of the sample (69.74 N and 850 rpm); (b) Percentage of heat fraction absorbed by the sample.

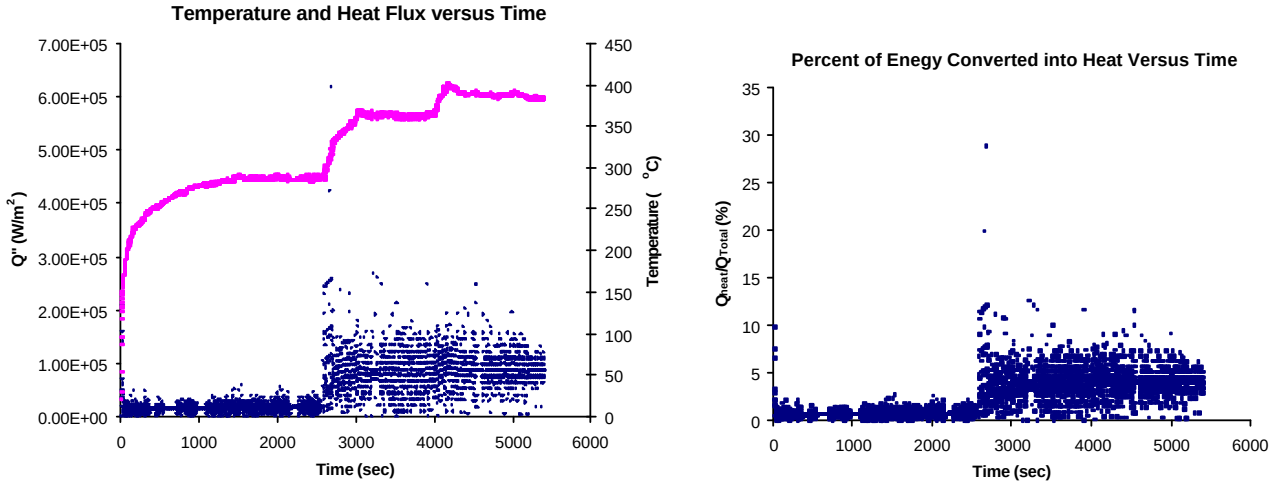

Figure 4. Finite element mesh of the model for temperature simulation

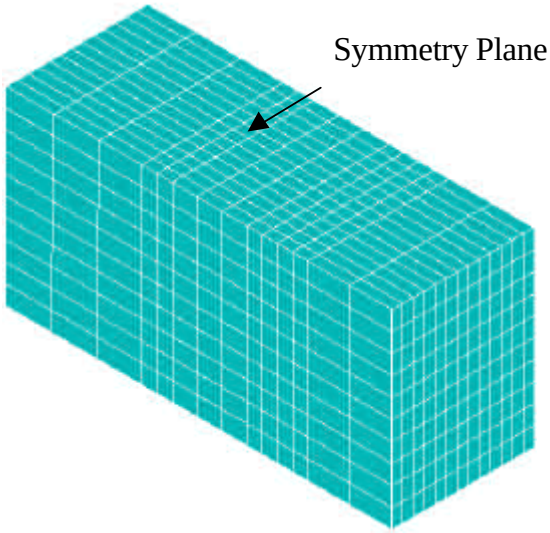

Figure 5. Simulation heat fluxes and temperature result from modeling.

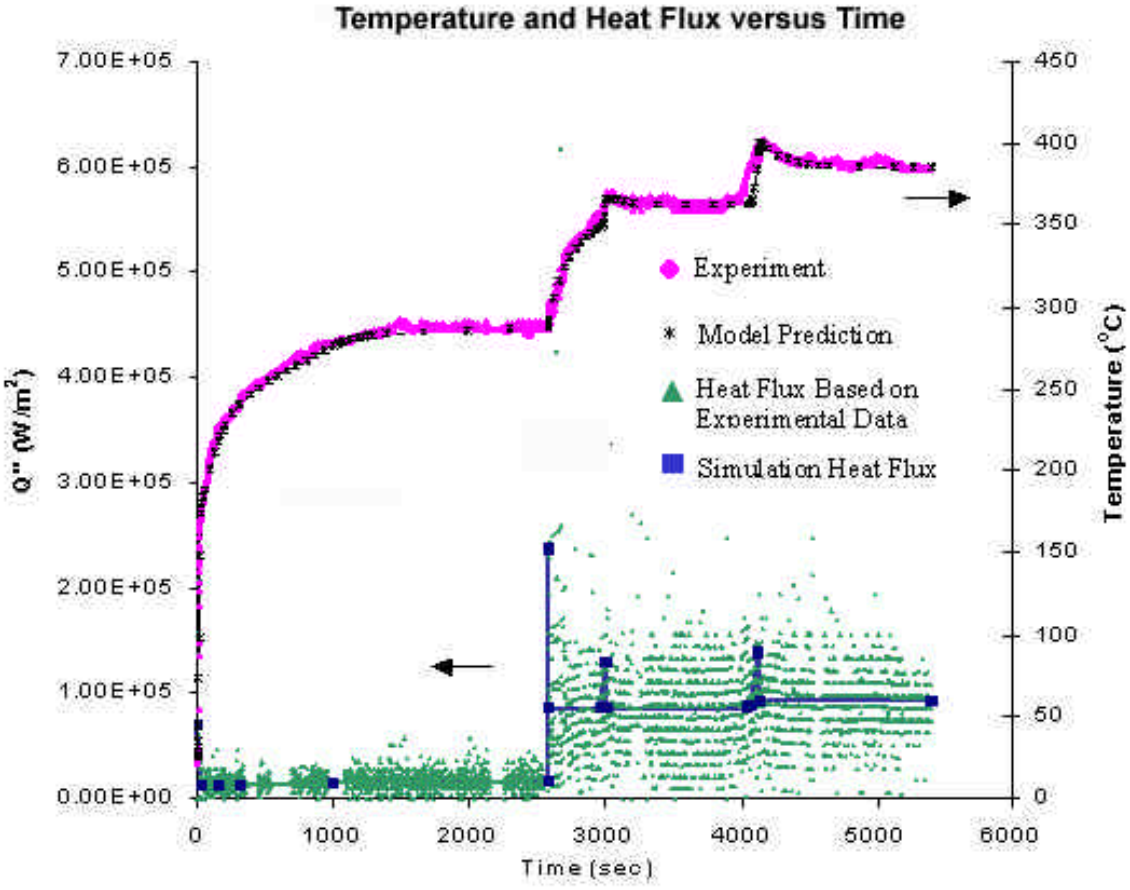

Figure 6. Temperature field of the sample from the modeling results.

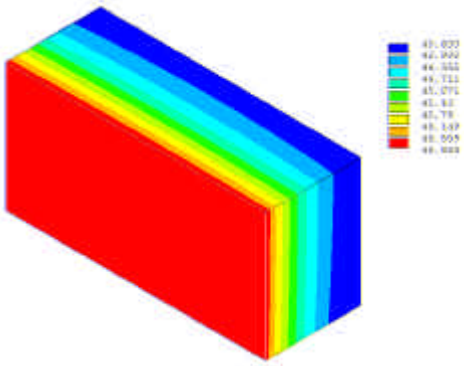

Time: 1.6 sec

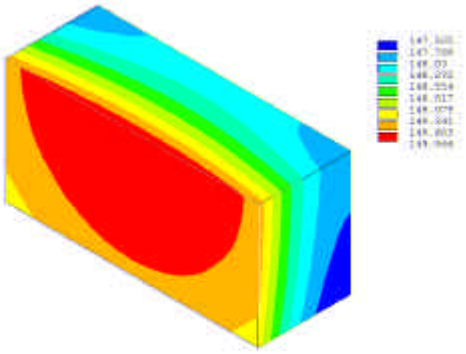

Time: 14.8 sec

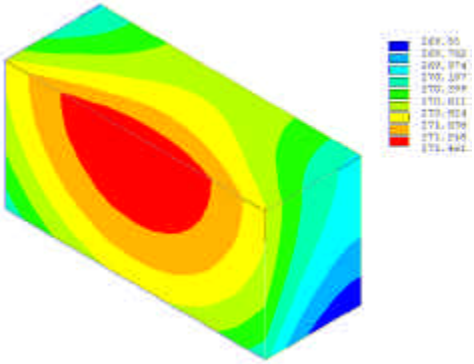

Time: 863 sec

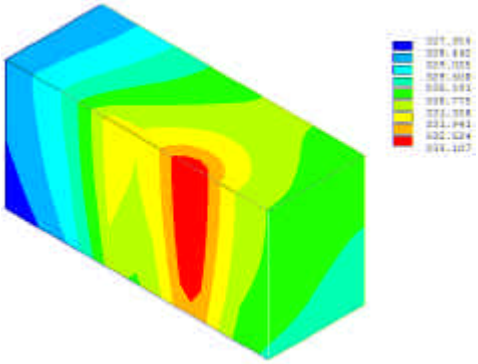

Time: 2737 sec (First Transition)

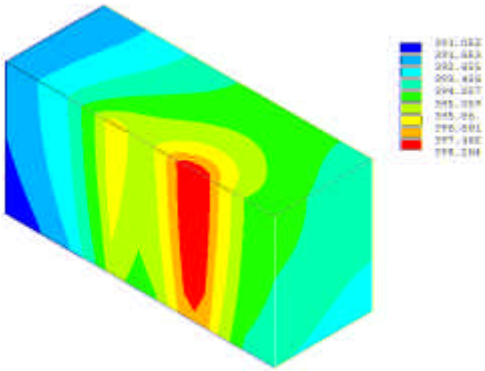

Time: 4070 sec (Second Transition)

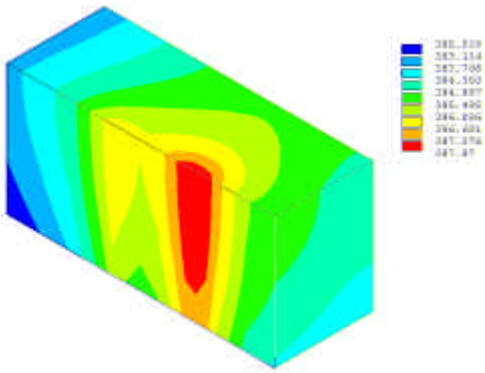

Time: 5200 sec

Figure 7. Mechanical properties of the sample as functions of temperature

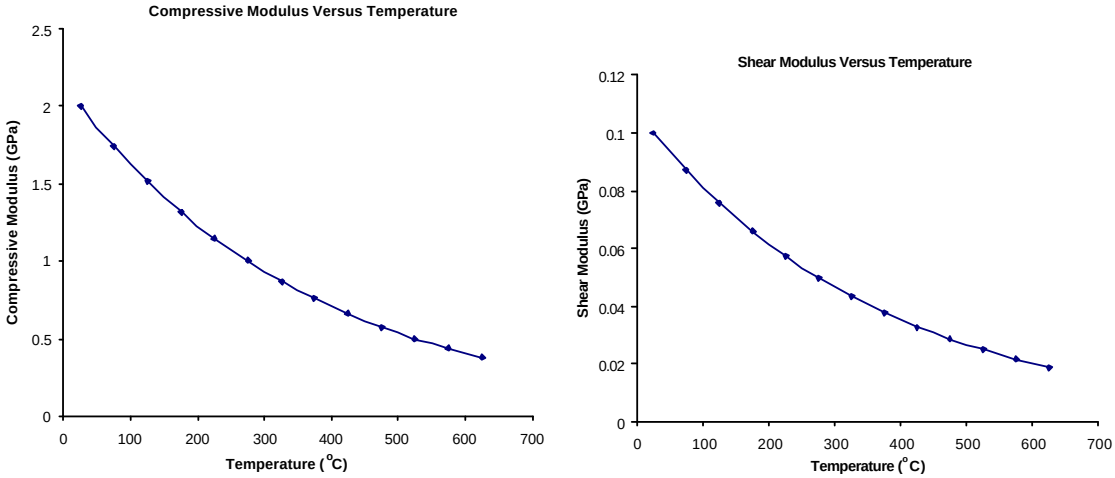

Figure 8. Normal force and friction coefficient as functions of time (69.74 N and 850 rpm).

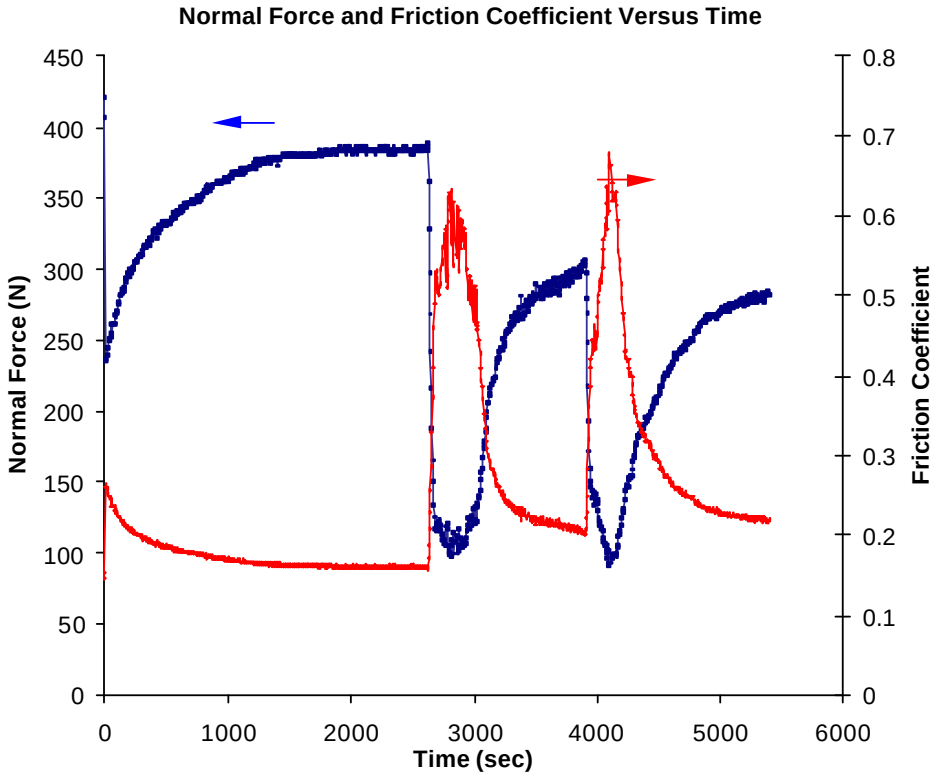

Figure 9. Simulated Von Mises stress field of the sample (Unit: MPa). Rubbing direction is indicated by the arrows.

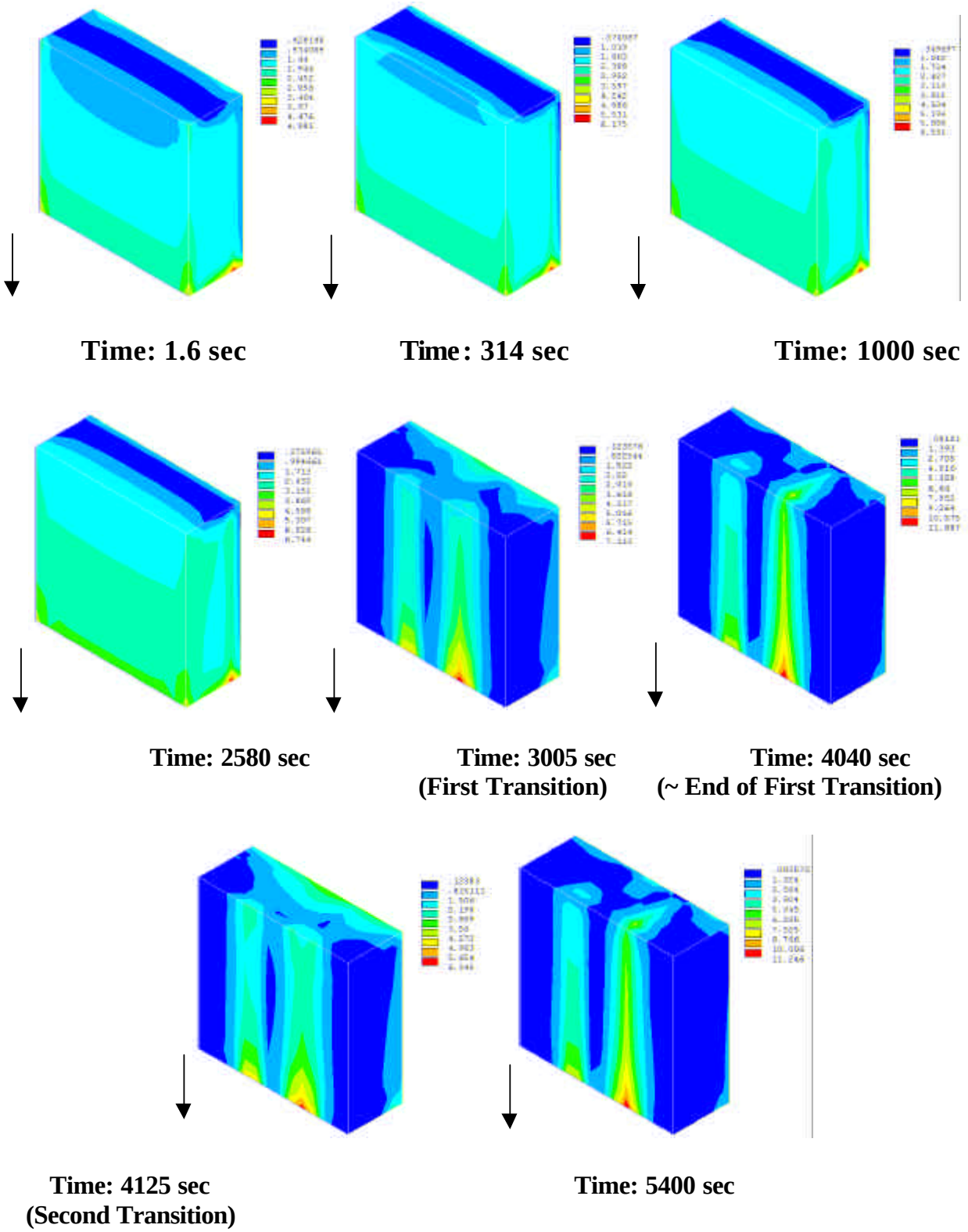

Figure10. Cracks generation in the samples of various testing conditions. The arrows indicate rubbing directions.